LA-UR- 98-2334

Approved for public release; distribution is unlimited.

Title: MULTISPECTRAL THERMAL IMAGING

CONF-980731--

Author(s): Paul G. Weber, NIS-2
Steven C. Bender, NIS-2
Christoph C. Borel, NIS-2
William B. Clodius, NIS-2
Alfred Garrett, Savannah River Tech. Center
R. Rex Kay, Sandia National Laboratory
Malcolm M. Pendergast, M. M. Pendergast Consultants
Barham W. Smith, NIS-2

Submitted to: SPIE Proceedings for the Imaging Spectrometry IV Conference,

19-24 July 1998

San Diego, CA

Los Alamos
NATIONAL LABORATORY

DISCLAIMER

DISCLAIMER

Portions of this document may be illegible in electronic image products. Images are produced from the best available original document.

V521

Multispectral Thermal Imaging

Paul G. Weber[a], Steven C. Bender[a], Christoph C. Borel[a], William B. Clodius[a], Alfred Garrett[c], R. Rex Kay[b]. Malcolm M. Pendergast[d], and Barham W. Smith[a]

[a] Space and Remote Sensing Sciences Group, Los Alamos National Laboratory, D436, Los Alamos, NM 87545.
[b] Monitoring Systems and Technology Center, Department 5700, Sandia National Laboratory, Albuquerque, NM 87185.
[c] Office A-1000, Savannah River Technology Center, Westinghouse Savannah River Corporation, Aiken, SC 29808.
[d] Formerly at SRTC, now at M. M. Pendergast Consultants, 3705 Pebble Beach Drive, Martinez, GA 30907

ABSTRACT

Many remote sensing applications rely on imaging spectrometry. Here we use imaging spectrometry for thermal and multispectral signatures measured from a satellite platform enhanced with a combination of accurate calibrations and on-board data for correcting atmospheric distortions. Our approach is supported by physics-based end-to-end modeling and analysis, which permits a cost-effective balance between various hardware and software aspects.

1. OBSERVABLES AND SIGNATURES

Many applications require observation of targets from a significant distance. The specific interests of the customers dictate the particular remote sensing systems that are deployed. For example, the NASA Mission To Planet Earth (MTPE) demands frequent global coverage to study environmental changes, including climate warming, rising sea level, deforestation, desertification, ozone depletion, acid rain, and reduction in biodiversity[1]. Conversely, others are interested in attributes of specific, smaller areas: for example, the Landsat[2] series of satellites image selected targets of up to 185 km swath width at spatial resolutions of 30 – 120 meters. Commercial interests are now developing satellite-based systems which have spatial resolutions down to one meter with commensurately smaller swath widths[3]. In addition to spatial and temporal resolution and coverage, and selection of spectral bands, each system has requirements for accuracy or precision, driven by the desired data products. The customer for the work described in this paper is interested in obtaining very accurate signatures from a variety of industrial sites. The observables include facility attributes (size, shape, materials), thermal signatures, and solid, liquid and gaseous effluents measured either directly, or by their effects on the environment as measured by, for example, vegetative health in the vicinity. Our goal is to develop and demonstrate advanced technologies and analysis tools toward meeting the needs of our customer; at the same time, the attributes of this system can address other applications in such areas as environmental change, agriculture, and volcanology.

We will concentrate first on measurement of thermal signatures, which can provide information on whether a facility is operating, and, if so, how much power is being dissipated. For example, consider an electrical power producing facility which uses water from an adjacent river for cooling. Typical plant efficiencies indicate that waste heat dissipation is twice the electrical power production: hence careful measurements of the waste heat provide useful data on electrical power production and on impacts to the environment. The thermal signature is manifest in infrared emissions, which may be measured by a suitable imaging system. However, the thermal signature is affected by the heat dissipation mechanisms, which, in turn, are affected by the state of the atmosphere. Also, the infrared signature is distorted by absorption and emission in the atmosphere between the river surface and the remote sensing system. Thus obtaining accurate retrievals at

ground level drives a design in which we can measure thermal and non-thermal scene attributes, as well as the variable aspects of the intervening atmosphere.

The analysis of the ground scene includes identification of materials, and evaluation of such properties as the health of vegetation. We rely here on the experience of many airborne and space sensors, including the AVIRIS[4] and HYDICE[5] hyperspectral sensors and the LandsatThematic Mapper[2] and SPOT[6] multispectral sensors, and on detailed modeling. It is clear from these efforts that, for a given spatial resolution and signal-to-noise, one obtains better separation of materials using more spectral bands. The data indicate that the spectral region from 0.4 to 2.5 microns provides the best "fingerprints" for the identification of solids and liquids; the thermal infrared is generally more appropriate for identification of gases. The key caveats here are on spatial resolution (which should be small to avoid confusion due to mixed pixels in a cluttered scene) and signal-to-noise (which, even for perfect detectors, will be limited by the available number of photons in the collecting aperture). Our goal here will be to reach the most appropriate solution for our customer's needs.

The atmosphere affects all of the listed signatures within the spectral range of interest. We can model these effects rather well, using sophisticated codes such as the U. S. Air Force sponsored MODTRAN[7], and the French 6S code[8]. However, atmospheric variability is significant, primarily in aerosols, water vapor, and cloudiness, on relatively small spatial and temporal scales. For example, data from AVIRIS shows water vapor varying on scales of tens of meters, and also shows considerable patchiness in clouds, including sub-visual Cirrus clouds. Time series data from weather stations show variability by factors of two or more between water vapor retrievals by balloon-borne weather-sondes launched at intervals of six hours. Three-dimensional mapping of water vapor distributions over uniform surfaces using Raman LIDAR shows cells with spatial scales of meters[9], and large gradients in the vicinity of vegetation[10]. Measurements of variability in column-integrated water vapor using microwave sensing similarly shows significant small-scale activity. Thus errors are introduced if the analyses rely exclusively on synoptic weather based on measurements by weather satellites at spatial scales of kilometers and at time scales of hours, combined with data from ground-based stations separated by tens of kilometers.

Thus our requirements are for a system with spatial resolution appropriate to examining industrial facilities, with spectral bands appropriate to the identification of facility attributes including thermal signatures, materials identification and effects on the nearby environment. These efforts constitute a technology demonstration, in which we plan to examine signatures from cooperative sites, and compare the results obtained by remote sensing to the attributes of the sites as determined by in-situ observations.

2. SYSTEM EMULATION AND DESIGN SOLUTIONS.

Physics-based end-to-end modeling and analysis.

We use sophisticated modeling and analysis tools to set appropriate specifications, and to predict and verify performance. The process is depicted in Figure 1. We begin by modeling multispectral signatures covering the visible and infrared parts of the spectrum (alternatively, we can use data from suitable airborne sensors). We propagate the signatures through representative atmospheres generally using the MODTRAN[7] or 6S[8] codes, which also add in the appropriate path radiance. This yields simulated spectra at the entrance aperture of our sensor. We model the sensor optical system using Code V[11] or with less sophisticated (but faster) methods such as propagation of the Point Spread Function (PSF) and the Modulation Transfer Function (MTF). The detectors are modeled[12] using fundamental physics, and data acquisition and control systems are modeled based on electronic engineering inputs. To complete the picture, we use the accuracy requirements for the final product (Answers to our customer's questions) to derive the requirements on calibration. This includes the transfer of calibration standards from the National Institute of Standards and Technology (NIST) via our ground calibration systems to the on-board calibration system for the sensor. We now iterate on this system to find the self-consistent solution that best meets our customer's needs.

The possible solutions need to be constrained by cost-effectiveness, and by a realistic evaluation of the uncertainties in the entire system. For example, it is not possible to achieve perfect calibration, and the atmospheric simulation codes have inherent disagreements with observations in such areas as matching the water vapor spectra. Our guiding principles include making the system reasonably simple, and finding a realistic balance in distributing the error budget. The full details of this process are beyond the scope of this paper, but the following discussion and references[13] provide an overview.

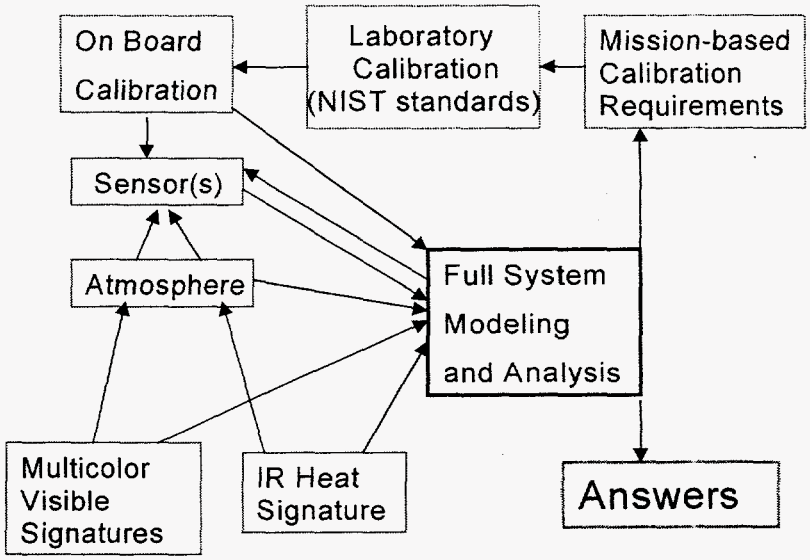

Figure 1.: Flow diagram for system design and implementation.

Wavelength selection.

We begin with selection of the wavelength bands. Our intent here is to find the minimal set which will address the range of signatures to be exploited, together with bands for corrections due to the atmospheric variability. Many more details of the selection processes for the bands are found in Clodius, Weber, Borel and Smith (1998).[14] The full spectrum received at the satellite consists of sunlight reflected from the atmosphere or from the Earth, plus thermal infrared emission from the Earth as modified and added to by the atmosphere. A typical spectrum is shown in Figure 2, which shows a representative full spectrum at the satellite aperture covering both reflected sunlight and thermal radiation. The crossover of these two components occurs in the MWIR. Selected spectral bands for the present design are superimposed.

Nighttime thermal retrievals, use the upper five bands of the ensemble, in two atmospheric "windows": nominally at 3-5 and at 8-12 microns. We chose to avoid the variable Ozone band at ~9.4 – 10 microns. We locate one band, designated band N, near the wavelength of peak radiance at 10.2 to 10.7 microns: this band is relatively unaffected by atmospheric effects. We add two bands, L and M, on the shorter wavelength side of the ozone feature, at 8.0 – 8.4 microns, and at 8.4 to 8.85 microns. Band M has a reasonably clear path to the ground while band L is affected by atmospheric water vapor: the ratio of these bands gives a measure of column integrated water vapor. We now complete our fit of the modified Planck curve with two bands in the Mid Wave Infrared (MWIR): band J at 3.50 – 4.10 microns and band K at 4.87 to 5.07 microns. The gap between these bands is dominated by the vibrational-rotational absorption band of CO_2 between ~4.2 and ~4.6 microns: as with the Ozone feature in the LWIR, we avoid the variable atmospheric components. Precedence for a satellite system exists for band J: for example, in the AVHRR (3.55 to 3.93 microns) and in the GOES Imager (3.80 to 4.00 microns)[15,16]. Band K is, to the best of our knowledge, new: it is affected by atmospheric composition, but is also essentially unaffected by the tail of the solar spectrum, thus making it a useful MWIR band during the day when band J is badly contaminated by sunlight. The combination of these five spectral bands, allows a powerful probing of the Planck curve as propagated to the satellite-borne sensor, correcting for atmospheric variables and obtaining excellent temperature retrievals on the ground.

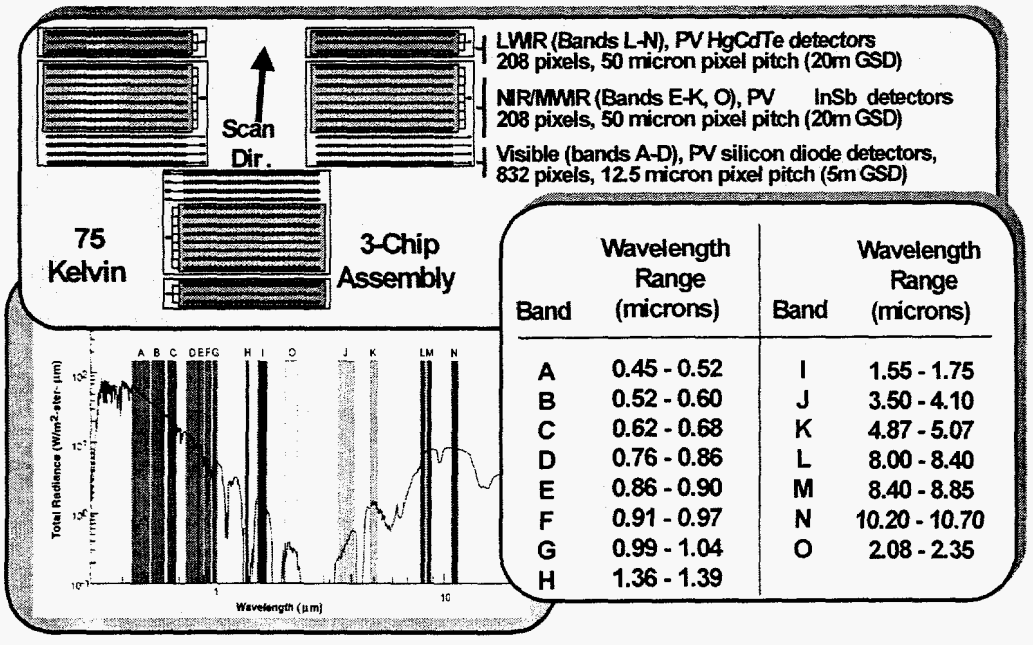

Band	Wavelength Range (microns)	Band	Wavelength Range (microns)
A	0.45 - 0.52	I	1.55 - 1.75
B	0.52 - 0.60	J	3.50 - 4.10
C	0.62 - 0.68	K	4.87 - 5.07
D	0.76 - 0.86	L	8.00 - 8.40
E	0.86 - 0.90	M	8.40 - 8.85
F	0.91 - 0.97	N	10.20 - 10.70
G	0.99 - 1.04	O	2.08 - 2.35
H	1.36 - 1.39		

Figure 2: Representative spectrum at the satellite, with chosen spectral bands superimposed, plus lay-out of the focal plane with three Sensor Chip Assemblies (SCAs) each with fifteen filtered linear array detectors.

During the daytime, we add information from the remaining ten spectral bands. Starting at short wavelengths, bands A-D are derivatives of the well-established Landsat bands, with some relatively minor modifications to reflect better technology and better understanding of where to best place the band edges. (We are quite unfettered with any requirement to provide operational continuous data streams, which allows experimentation.) These four bands are used in materials identification, vegetation health (as measured by MDVI) and to assess the aerosols from the Rayleigh scattering effects.

The next three bands, E, F, and G, encompass the water vapor absorption feature at around 0.94 microns. Following AVIRIS analysis[17,18] one can take ratios of these bands to directly map the column integrated water vapor over most target scenes (one experiences difficulties with low emissivity targets). This method has been extended by Borel, *et al*[19,20] in a method called: "Atmospheric Pre-corrected Differential Absorption".

Further consideration of AVIRIS hyperspectral VNIR data shows the ability to detect even sub-visual cirrus clouds using a strong water vapor absorption at 1.375 microns[21]: we chose to define this as a single spectral band. Our next two bands also are Landsat derivatives: band I at 1.54 – 1.75 microns is well known for vegetation / lignin retrievals, and our band O at 2.08 – 2.35 microns provides needed discrimination for separation of certain materials.

Spatial sampling and coverage.

We gain significant information from the ability of the satellite to maneuver over a range of +/- 20 degrees across the track and almost horizon to horizon in the along-track direction. This permits stereo imaging, and also allows us to observe the same ground scene through different segments of the atmosphere. Assuming a laminar atmosphere, this permits superior atmospheric corrections than are possible with only a single view. In a non-uniform atmosphere it permits, for example, discrimination of clouds based on perspective changes (in addition to the usual spectral discrimination).

Spatial resolution is limited, *inter alia*, by the diffraction limit of the telescope. Using a nominal 500-km altitude for the satellite, we compute the diffraction limit at the wavelength peak of the Planck curve for thermal emission from objects with temperatures near Earth-ambient values. At a nominal ten microns wavelength, a 0.36 m diameter primary aperture gives a diffraction limited spot of 34 meters: numerical studies demonstrate that this is adequate for a good selection of lake, river, or ocean cooling systems associated with typical power plants. If the telescope were to be diffraction limited at all wavelengths, this would imply a diffraction limit of less than two meters in the visible spectrum, which is better than we require for the subject applications.

The spatial coverage can be rather modest, since we will be targeting cooperative sites whose location is well known to us. The satellite will have three reaction wheels, which provides pointing control to an accuracy of 2 km at 98 percent confidence. Thus, even large facilities will be almost guaranteed to be in the field of view if we have a swath of, say, 5 km, and we can demonstrate limited area search capabilities with a swath of, say, 12 km. We targeted the larger swath for the optical system, which leads to a field of view of 1.4 degrees.

Taking the 0.36-meter diameter primary mirror, and a reasonable f-stop of 3.5, we have an effective focal length of 1.25 meters. We chose a non-obstructed telescope, since any obstructions would impair our ability to reach our calibration goals (unless we spent a great deal of effort in controlling the obstructing hardware in terms of temperature, emissivity, scattering, etc.). We also wanted to be able to make in-flight focus adjustments, and have both full aperture and local on-board calibration systems. A Three Mirror Anastigmat (TMA) design proved to be an appropriate solution to these requirements.

Our next task is to match the focal plane and pixel sizes to the telescope. The focal surface of the TMA is computed to be quite flat, and has dimensions of 30.7 x 43.2 mm. Again we start with the longest wavelengths in the system, and find that HgCdTe is the detector material of choice (high QE, cooling requirement of around LN2 temperatures, and good yield in production of linear arrays containing up to a few hundred pixels). Available detector sizes of a nominal 50 microns permit near-Nyquist sampling at the longest wavelengths, for a Ground Sampling Distance (GSD) of a nominal 20 meters. The MTF at the Nyquist frequency is 0.64 for this band. For simplicity in the focal plane, we choose to maintain the nominal 50-micron pixel size for all spectral bands used in thermal analysis and in atmospheric retrievals. For the four bands in the visible and near infrared, we recall a potential for a diffraction limit of less than two meters. However, Nyquist sampling over the full available 12 km swath would then imply 12,000 detector elements per array, with detectors of around two micron pixel dimensions. This strains producibility capabilities, and would lead to a very large load on the data acquisition system. Thus we degraded the ground sampling distance for these bands to five meters, using nominal 12.5 micron pixels in relatively easy to produce silicon linear arrays of 832 elements each. Again for reasons of producibility, the Focal Plane Array (FPA) is split into Sensor Chip Assemblies (SCAs), each containing fifteen parallel

filtered linear arrays oriented at ninety degrees to the satellite direction of travel (i.e. a "push-broom" configuration). Three such SCAs cover the 12-km swath.

A Stirling Cycle cooler can maintain the entire focal plane at an operating temperature of 70K. This is necessary for low-noise operation of the infrared detectors. The VNIR detectors could be operated at a higher temperature, but this would require a beam splitter in the field of view of the IR sensors, which would likely reduce the temperature accuracy of the system. A set of cold baffles is used to minimize the coupling of the warm structure to the FPA, and to reduce stray light. The maximum FPA thermal load is 2.25 Watts, which requires over 100 Watts of primary electrical power to the cooler. The remainder of the optical system is carefully maintained at a monitored space-ambient temperature of 270 - 275K: thus the background radiance from the telescope is known and can be subtracted from the measured signals.

Error budget and calibration.

The system error budget is divided almost equally between the hardware and the analysis uncertainties. This balance leaves challenging, state-of-the-art assignments in both areas, with confirmation of actual on-orbit performance from measurements made on well-characterized ground-based scenes. The hardware calibration requirements flow from the end-to-end modeling to on-orbit requirements on the accuracy of each spectral band. Each band has a different set of specifications, and again the details are beyond the scope of this paper. However, we will illustrate the sequence in the following paragraphs.

The reference source for all calibrations is the National Institute of Science and Technology (NIST). The goal of the calibration is to transfer NIST standards to the satellite instrument, and then to maintain the calibration for the life of the system. The preferable approach to translating between the NIST sources and the satellite instrument is to use a telescope to expand from the small sources to the full aperture of the instrument. This is achieved at Los Alamos in the Radiometric Calibration System (RCS) using a two mirror telescope with a full aperture of ~0.5 meters diameter. The secondary mirror of that telescope can be rotated at an angular rate equal to the satellite imaging rate in orbit; this allows a full, dynamic simulation of the on-orbit operations.

We have worked directly with NIST to develop new transfer sources for broadband visible and infrared. These sources must be operated in vacuum, and are located at the focal point of the telescope whose output provides full aperture illumination of the instrument. The VNIR source is an integrating sphere with nitrogen gas cooling used to dissipate the heat of the lamps. Two blackbody sources have been developed to cover the temperature range 180 – 350K with temperature control of better than 50 mK. and an effective emissivity of 0.998 +/- 0.002[22]. The small blackbody and the integrating sphere sources have been directly calibrated at NIST, and can be used directly as sources, or can be used to illuminate targets which can be used to test alignment and the MTF of the full system. The final source in the Radiometric Calibration System (RCS) is the output of a double monochromator to check wavelength responses.

The satellite payload features two calibration systems, as depicted in Figure 3. At the entrance of the optical system, we have a clamshell door, which is normally closed to maintain thermal stability. The inner surface of the door is high emissivity black, and is temperature controlled to provide full-aperture infrared calibration of the entire system. The clamshell can be partially deployed, which presents a diffuser surface (Z-93 paint) to incoming solar radiation. The output of the diffuser can provide a full aperture VNIR/SWIR calibration of the system, or the output can be directed into a small filtered cavity radiometer to check for degradation of the diffuser surface. Near the focal plane we have located a quick look calibration wheel with two blackbodies, a two-level integrating sphere, a gold surface retro mirror and an open aperture. The wheel is in a protected location, but provides calibration data only for the FPA and associated hardware. Each of these on-board calibration sources is to be calibrated against the highly accurate output of the RCS, thus providing full traceability to NIST standards. The combination of these calibration systems will provide unprecedented on-board calibration capability.

System configuration.

The launch configuration for the system is approximately a cylinder, 1.35 m in diameter and 2.6 m long with a total mass of 625 kg, requiring a Taurus or similar launch vehicle to reach Low Earth Orbit of nominally 500 km. Once in orbit, four solar paddles deploy, and three reaction wheels are used to keep the solar paddles pointed at the Sun, maximizing power generation. For imaging the system proceeds through a calibration sequence, sweeps across the target site, takes one or more images, repeats the calibration sequence and then resumes the sun-pointing orientation. Peak power during imaging is 800 Watts, and the peak data rate is ~400 Mbits/second to an on-board store and forward memory whose content is linked down to the ground station several times per day.

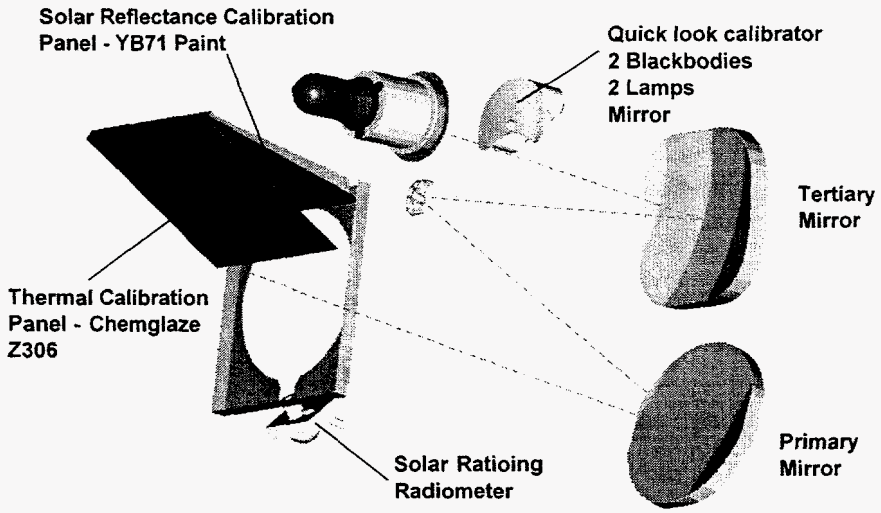

Figure 3: Depiction of the major elements of the on-board calibration systems.

Data analysis is based on the analysis segments of the end-to-end model. The first step involves re-registration of the fifteen spectral bands on three SCAs to form images: some new techniques in this area have recently been presented. Calibrations will need to synthesize data from a number of sources: on-board calibration systems, reference to calibrated ground targets, celestial objects and deep space. However, we expect to spend most of our efforts in translating the multispectral data into useful data products following atmospheric corrections. Standard products include[23,24]: image sharpening and restoration, temperature retrievals, materials identification, vegetative stress, atmospheric state, etc. Community experts have recently reviewed plans for the algorithms.

The ultimate test of the system will be in comparing the information retrieved from on-orbit measurements to well-characterized targets. These targets include lakes, rivers, oceans, relatively uniform solids such as desserts or dense vegetation, and a variety of man-made targets. Appropriate ground truth activities will be conducted, either separately or in collaboration with other systems.

3. SUMMARY

We have described a physics-based approach to the design of a multispectral thermal imaging mission. We employ end-to-end modeling to support trade studies, evolving to a system which meets customer needs with reasonably available technologies. We divide the error budget between hardware and analysis, thus providing a challenging, but achievable, set of goals in each area.

4. ACKNOWLEDGEMENTS

The US Department of Energy supports this work at Los Alamos National Laboratory, Sandia National Laboratory, and the Savannah River Technology Center. The authors are very grateful to their colleagues who contribute to the work described in this paper, and to the management of their Laboratories for their support.

5. REFERENCES

1. G. Asrar and R. Greenstone (eds), "1995 MTPE/EOS reference handbook", NASA (1995).

2. E. J. Sheffner, "The Landsat program: Recent history and prospects", Photogrametric Engineering and Remote Sensing, pp 735-744 (199X).

3. A concise summary is found in: M. Felsher, NASA-FEMA Conference on GIS and Applications of Remote Sensing to Disaster management, NASA GSFC 13 January 1997 (1997).

4. R. O. Green (Ed): "Annual JPL Airborne Geosciences Workshops", NASA JPL (1993-1998)

5. R. W. Basedow, D. C. Carmer and M. E. Anderson, Proc. SPIE, Vol 2480, 258 (1994).

6. See the WWW pages at www.spot.com.

7. L. W. Abreu, J. H. Chetwynd, G. P. Anderson and L. M. Kimball, "MODTRAN 3 Scientific Report, Geophysics Laboratory, US Air Force, Hanscom AFB, MA.

8. E. Vermote, D. Tanre, J. L. Deuze, M. Herman and J. J. Morcette, "Second Simulation of the Satellite Signal in the Solar Spectrum" NASA GSFC (1994).

9. D. I. Cooper, W. E. Eichinger, R. E. Ecke, J. C. Y. Kao, J. M. Reisner and L. L. Tellier, "Initial investigations of microscale cellular convection in an equitorial marine atmospheric boundary layer revealed by lidar" Geophysical Research Letters, Vol 24, pp 45-48 (1997).

10. D. I. Cooper, Los Alamos National Laboratory, Private communications (1997 and 1998).

11. Optical Research Associates, 3280 East Foothills Boulevard, Pasadena, CA 91107.

12. B. J. Cooke, B. E. Laubscher, C. C. Borel, T. S. Lomheim and C. F. Klein, "Methodology for rapid infrared multispectral electro-optical imaging system performance analysis and synthesis", SPIE Conference on Infrared Imaging Systems: Design, Analysis, Modeling and Testing VII, 10-11 April 1996, Orlando, Florida, Proc. SPIE Vol 2743, pp 52-86(1996).

13. B. W. Smith, C. C. Borel, W. B. Clodius, J. Theiler, B. E. Laubscher and P. G. Weber, "End-to-end performance modeling of passive sensing systems", Proc. SPIE Vol. 2743, pp285-289 (1996).

14. W. B. Clodius, P.G. Weber, C. C. Borel and B. W. Smith, "Multi-spectral band selection for satellite-based systems", SPIE Conference on Imaging Systems: design, Modeling and testing IX, 15-16 April 1998, Orlando, Florida, to be published in Proc. SPIE Vol 3377, paper 3377-02 (1998).

15. P. K. Rao, S. J. Holmes, R. K. Anderson, J. S. Winston, and P. E. Lehr (eds), "Weather satellites: systems, data, and environmental applications", American Meteorological Society, Boston (1990).

16. H. J. Kramer, "Observation of the Earth and its environment", Springer-Verlag , New York (1994).

17. R. O. Green, V. Carrere and J. E. Conel, 'Measurement of atmospheric water vapor using the airborne visible / infrared imaging spectrometer" in Am. Soc. Photogrametry And Remote Sensing Workshop on Image Processing, Sparkes, NV 23-26 May 1989 (1989).

18. B. –C Gao and A. F. H. Goetz, "Column atmospheris water vapor and vegetation liquid water retrievals from airborne imaging spectrometer data", JGR Vol 95, D4, pp 3549 – 3564 (1990).

19. C. C. Borel, W. C. Clodius and J. Johnson, "Water vapor retrieval over many surface types", SPIE Conference on Algorithms for Multispectral and Hyperspectral Imagery II, 9-11 April 1996, Orlando, Florida, Proc. SPIE, Vol 2758, pp 218-228 (1996).

20. C. C. Borel and D. Schlapfer, "Atmospheric Pre-corrected Differential Absorption techniques to retrieve columnar water vapor: Theory and Simulations", Annual JPL airborne science workshop, 4-6 March 1996, Pasadena, California, NASA/JPL (1996).

21. B.–C Gao and A. F. H. Goetz, "Cirrus cloud detection from airborne imaging spectrometer data using the 1.38 um water vapor band" Geophysical Research Letters Vol 20, pp301-304 (1993).

22. D. A. Byrd, F. D. Michaud, S. C. Bender, et al, "Design, manufacture and calibration of infrared radiometric blackbody sources", SPIE Conference on Aerospace Defense Sensor and Control, 8-12 April 1996, Orlando, Florida, Proc. SPIE Vol 2743, pp 216-226 (1996).

23. J. Theiler, B. G. Henderson and B. W. Smith, "Algorithms using inter-band cross-correlation for pixel registration and jitter reconstruction in multi-channel push-broom imagers", Proc. SPIE, Vol 3163, pp 22-32 (1997).

24. B. G. Henderson, C. C. Borel, J. P. Theiler and B. W. Smith, "Image quality degradation and retrieval errors introduced by registration and interpolation of multispectral digital images". SPIE Conference on Signal and Data Processing of Small Targets, 9-11 April 1996, Orlando, Florida, Proc. SPIE, Vol 2759, pp 149-160 (1996).

For further information, contact: Paul G. Weber, Group Leader, Space and Remote Sensing Sciences, MS D436, Los Alamos National Laboratory, Los Alamos, NM 87545, phone: (505) 667-5776, Facsimile: (505) 665-4414, e-mail: pweber@lanl.gov or visit related WWW pages starting at: www.lanl.gov